Supplementary Information for

Ultra-flexible organic light-emitting diodes for optogenetic nerve stimulation

Dongmin Kim[1], Tomoyuki Yokota[1], Toshiki Suzuki[1], Sunghoon Lee[1], Taeseong Woo[1], Wakako Yukita[1], Mari Koizumi[1], Yutaro Tachibana[1], Hiromu Yawo[2], Hiroshi Onodera[1], Masaki Sekino[1,*], and Takao Someya[1,*]

[1]Department of Electrical Engineering and Information Systems, Graduate School of Engineering, University of Tokyo, 7-3-1 Hongo, Bunkyo-ku, Tokyo 113-8656, Japan.
[2]Department of Developmental Biology and Neuroscience, Graduate School of Life Sciences, Tohoku University, 2-1-1 Katahira, Aoba-ku, Sendai 980-8577, Japan.

[*]Corresponding authors: someya@ee.t.u-tokyo.ac.jp and sekino@bee.t.u-tokyo.ac.jp.

This PDF file includes:

- Supplementary text
- Figures S1 to S12
- Tables S1
- Legends for Movies S1 to S3
- SI References

Other supplementary materials for this manuscript include the following:

- Movies S1 to S3

www.pnas.org/cgi/doi/10.1073/pnas.2007395117

Supplementary Information Text

Theoretical evaluation of MRI compatibility of an OLED device

A conductive medium attenuates the incident electromagnetic wave, as shown in fig. s8a, and the attenuation coefficient α is given by

$$\alpha = \sqrt{\pi f \mu_0 \sigma} \qquad (1)$$

where μ_0 is the permeability of free space, f is the frequency of the incident wave, and σ is the conductivity of the medium. The skin depth δ_s is then given by

$$\delta_s = \frac{1}{\alpha} = \frac{1}{\sqrt{\pi f \mu_0 \sigma}}. \qquad (2)$$

The evaluation of MRI compatibility of the OLED device is based on the amount by which the radio-frequency wave mediating MRI signals penetrates into the medium.

The Larmor frequency of the 7-T MRI system is 300 MHz. Assuming the conductivities of gold, aluminum, and ITO to be 4.1×10^7, 3.5×10^7, and 1.0×10^6 S/m, the resulting attenuation coefficients are 2.2×10^5, 2.0×10^5, and 3.4×10^4 $\mathrm{Np\cdot m^{-1}}$, respectively. The ratio of the attenuated field amplitude to the incident amplitude is plotted in fig. s8b for various thicknesses of the medium. The estimated skin depths of the gold, aluminum, and ITO layers were calculated using equation (2) to be 4.5, 4.9, and 29 μm, respectively. The gold layer of the OLED device was fabricated with a thickness of 100 nm. This is 1/45 the skin depth of gold. The electric field of the incident wave was calculated to attenuate by 2.2% because of the gold layer. The aluminum layer, with a thickness of 200 nm, was 1/25 its skin depth. This caused the electric field to attenuate by 4.0%. Because of its lower conductivity, the ITO layer was fabricated with a thickness of 70 nm, 1/414 its skin depth. The electric field attenuated by 0.3% through this layer.

The amplitude of the attenuated wave resulting from the two-layered gold and ITO structure is given by

$$|E_{xo}| = \left(|E_{xi}| e^{-\alpha_{gold} t_{gold}}\right) e^{-\alpha_{ITO} t_{ITO}} \qquad (3)$$

where α_{gold} and α_{ITO} are the attenuation coefficients of gold and ITO, respectively. t_{gold} and t_{ITO} denote the thicknesses of the gold and ITO layers. In this case, the intensity is estimated to attenuate by 2.5% in the 7-T MRI.

Bending stiffness of OLED device for large-area illumination

To attach a uniformly flexible device (fig. s12a) of bending stiffness EI and width w to a model tissue with a radius of curvature R, the adhesion energy γ per unit area is given by the following equation (13):

$$\gamma = \frac{EI}{2R^2 w} \qquad (4)$$

In the case of rigid elements implemented on a flexible substrate, only the flexible part bends to conform to the curving surface, as shown in fig. s12b. As a result, the radius of curvature becomes smaller compared to the uniformly flexible device. Assuming the respective lengths of flexible and rigid components are a and b, as shown in fig. s12c, the radius R' of the flexible part has to satisfy the following equation:

$$R - R' = \frac{b}{2\tan\left(\frac{a}{2R'}\right)}. (5)$$

When *R* is sufficiently larger than *a* and *b*, *R′* can be simplified to

$$R' = \frac{R}{1+\frac{b}{a}} . \qquad (6)$$

The adhesion energy *γ′* per unit area of the flexible part can then be calculated as

$$\gamma' = \frac{EI}{2R^2 w}\left(1+\frac{b}{a}\right)^2 = \gamma\left(1+\frac{b}{a}\right)^2 . \qquad (7)$$

In this case, the effective bending stiffness is larger than that of the uniformly flexible device. This indicates that greater stress is induced in the flexible part. The average adhesion energy per unit area is given by

$$\gamma_w = \frac{a}{a+b}\gamma_f = \left(1+\frac{b}{a}\right)\gamma . \qquad (8)$$

This equation specifies the increase in adhesion energy. A light source in a uniformly flexible device illuminates a large curving surface with lower bending stiffness and adhesion energy than an array of rigid light sources.

Fig. S1. Structure and characteristics of the OLED device. (**A**) Left photo shows that the OLED device has extraordinary flexibility because of its thickness of only 2 μm. Right illustration shows the two-layered wiring structure which consists of a supporting gold layer on the ITO layer. The gold layer was patterned only outside the light-emitting area. Scale bar: 5 mm. (**B**) The normalized light power versus the input driving power for the two-layered wiring compared with the one-layered wiring made from ITO. The light power of the one-layered OLED was saturated, and the device degraded at above 1000 mW. The light power of the two-layered OLED exceeded this saturated light power at the input power of 500 mW. (**C**) Photograph of the OLED placed on a razor blade. The OLED emits light even when it is bent sharply. Scale bar: 2 mm. (**D**) The I-V characteristic was measured with pulsed voltages with amplitudes from 5 to 20 V, pulse duration of 5 ms, and at a frequency of 2Hz. (**E**) Distribution of light output from the OLED with angle. (**F**) The dependence of luminance on the driving voltage (L–V). (**G**) Distribution of luminance in 2 mm × 2 mm area of the OLED cell. (**H**) Normalized luminance as a function of time.

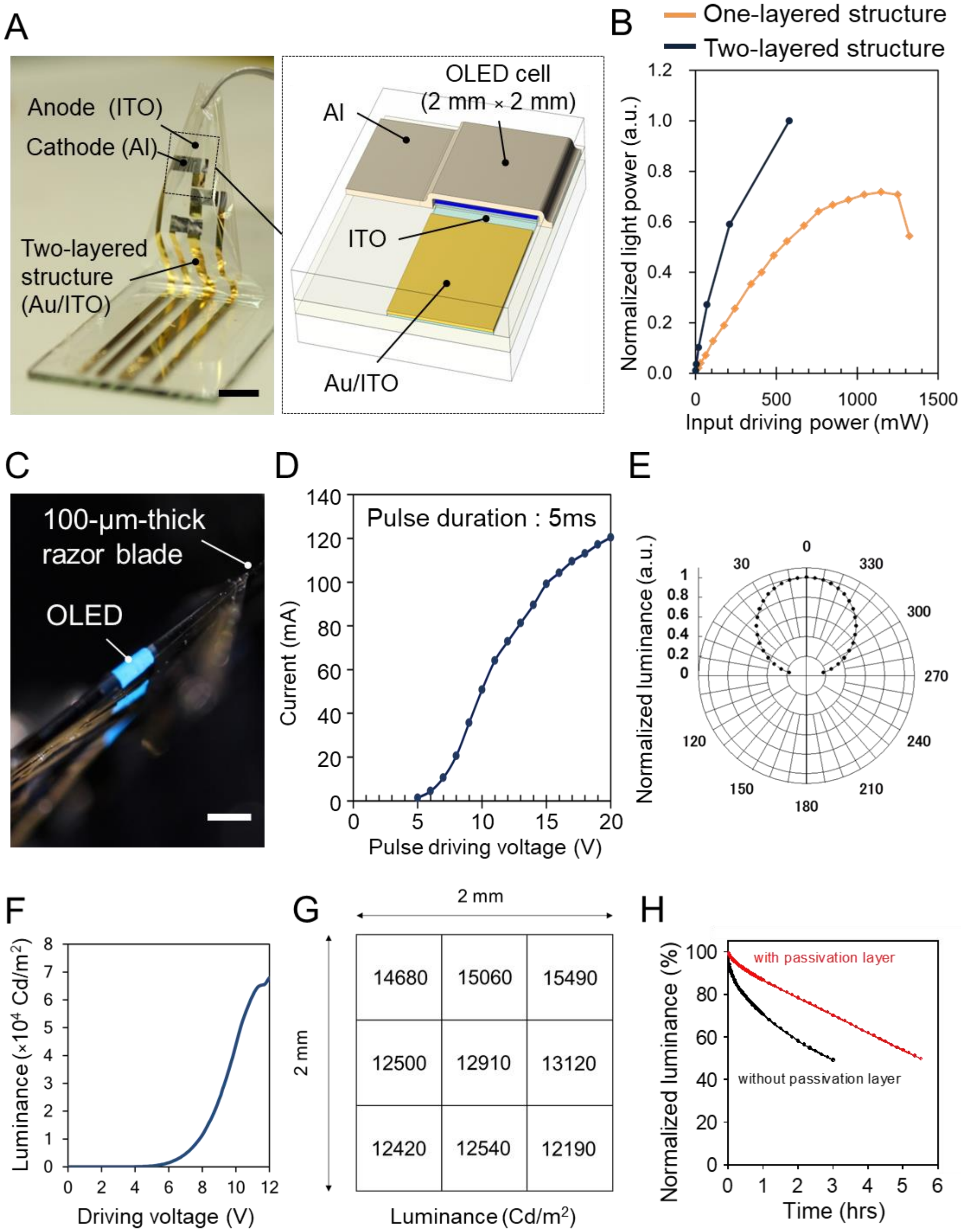

14680	15060	15490
12500	12910	13120
12420	12540	12190

Fig. S2. The lifetime of the OLED under the operating conditions. (**A**) The top photograph shows the experimental setup for measuring lifetime of the OLED in ambient condition (25ºC, 40%). The bottom photograph shows the OLED on an extracted thigh muscle tissue with the thickness of 2 mm. The OLED was driven with pulses of 15 V and 5 ms duration at 2 Hz. The change of light intensity was measured using a photodiode (VTB8440BH, Excelitas Technologies, USA). (**B**) The lifetime of the OLED under the operating conditions of animal experiments. An extracted muscle tissue was placed on the OLED to investigate the effect of moisture.

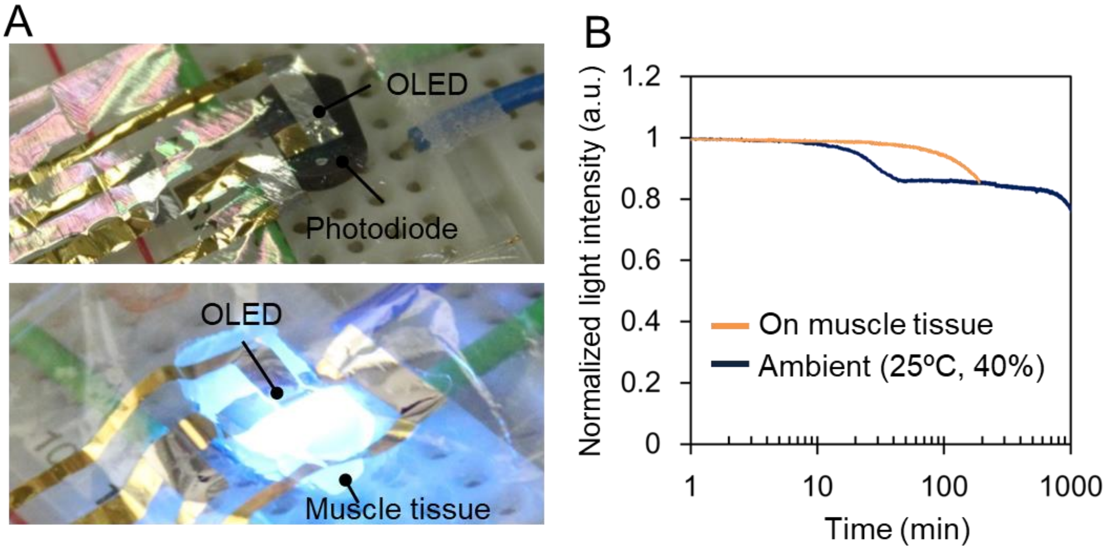

Fig. S3. Optical stimulation of nerves on gracilis muscle. (**A**) The OLED device attached to the gracilis muscle. To record electromyograms evoked by optical stimulation, a pair of needle electrodes was inserted into the muscle. Scale bar: 5 mm (**B**) **I**-V characteristics measured before and after attaching the OLED to the muscle. (**C**) The electromyogram decreases under high-frequency stimulations of 20 and 40 Hz due to the desensitization of channelrhodopsin-2. (**D**) Leakage current from the contacted OLED device on the muscle.

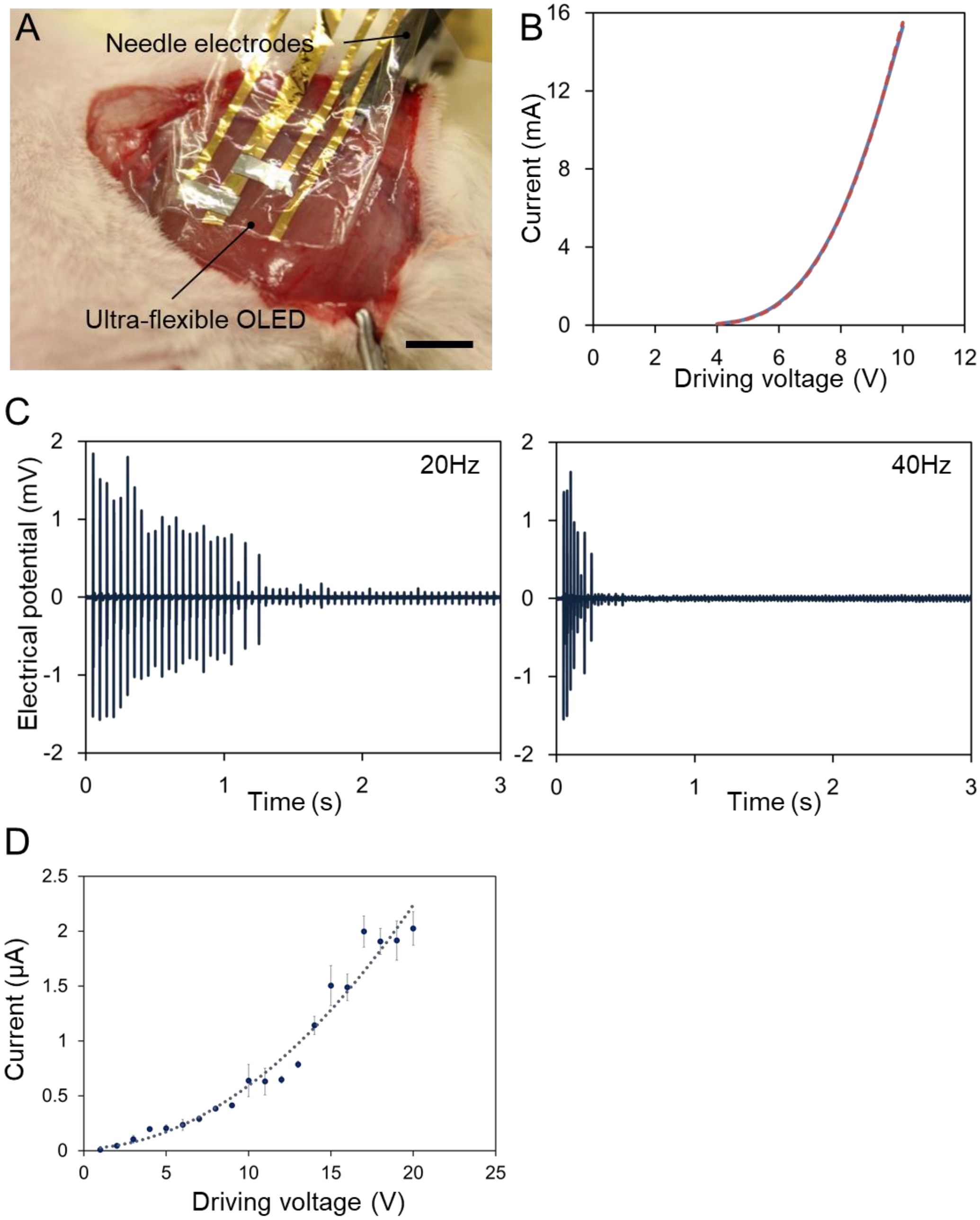

Fig. S4. Evaluation of thermal effect on activation of nerve. (**A**) Photograph of 580 nm laser coupled optical stimulation on a sciatic nerve fiber. (**B**) Heating effects on tissues by illuminating using 470 nm laser at 3.2 mW and 580 nm laser at 3.6, 7.5 and 11.2 mW. The laser was illuminated from 60 to 90 s (a duration of 30 s) and the temperature changes were measured using a thermocouple positioned on the tissue surface at ~ 200μm from the tip of the optical fiber. (**C**) Evoked electromyograms at the gastrocnemius muscle by the above conditions of laser stimulation. The 580 nm laser did not induce muscle contraction even at intensities as strong as 11.2 mW. (**D**) Evoked electromyograms at the gastrocnemius muscle of a wild type rat by the above conditions of laser stimulation.

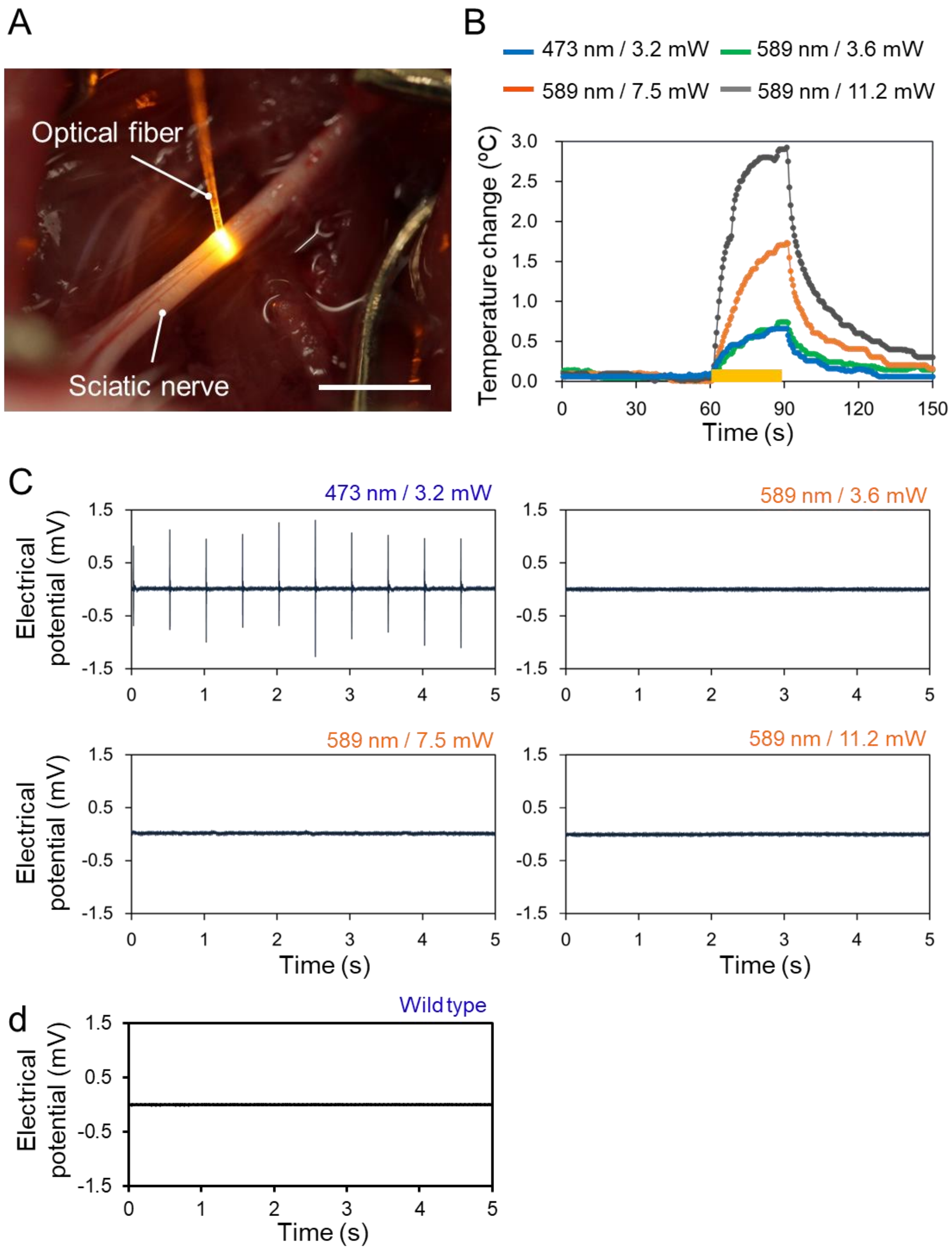

Fig. S5. Somatosensory evoked potentials (SEPs) obtained by electrical stimulation of a hindpaw. (**A**) Dependence of SEPs on current intensities ranging from 0.3–0.7 mA. (**B**) The peak has a longer latency and lower amplitude under a smaller stimulating current.

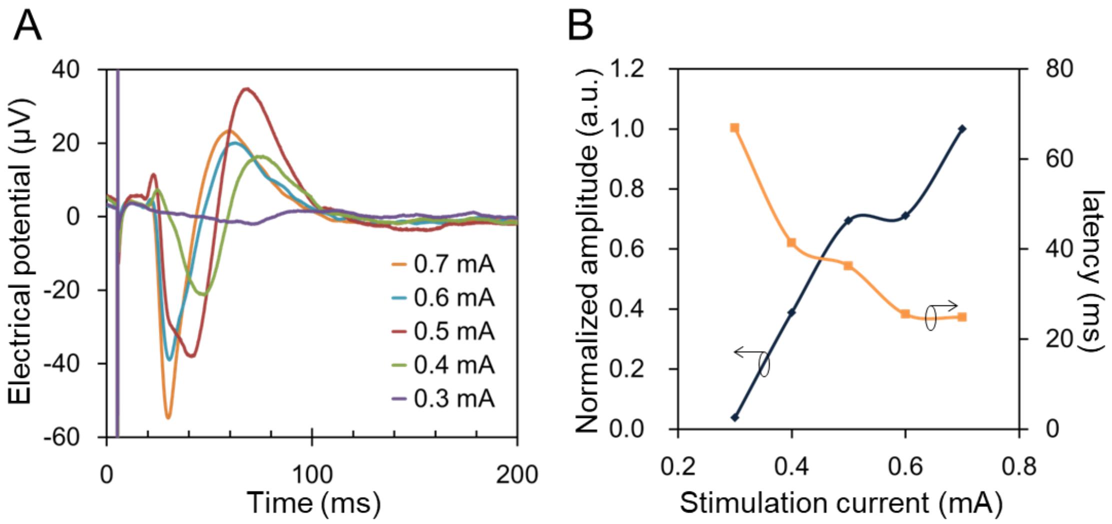

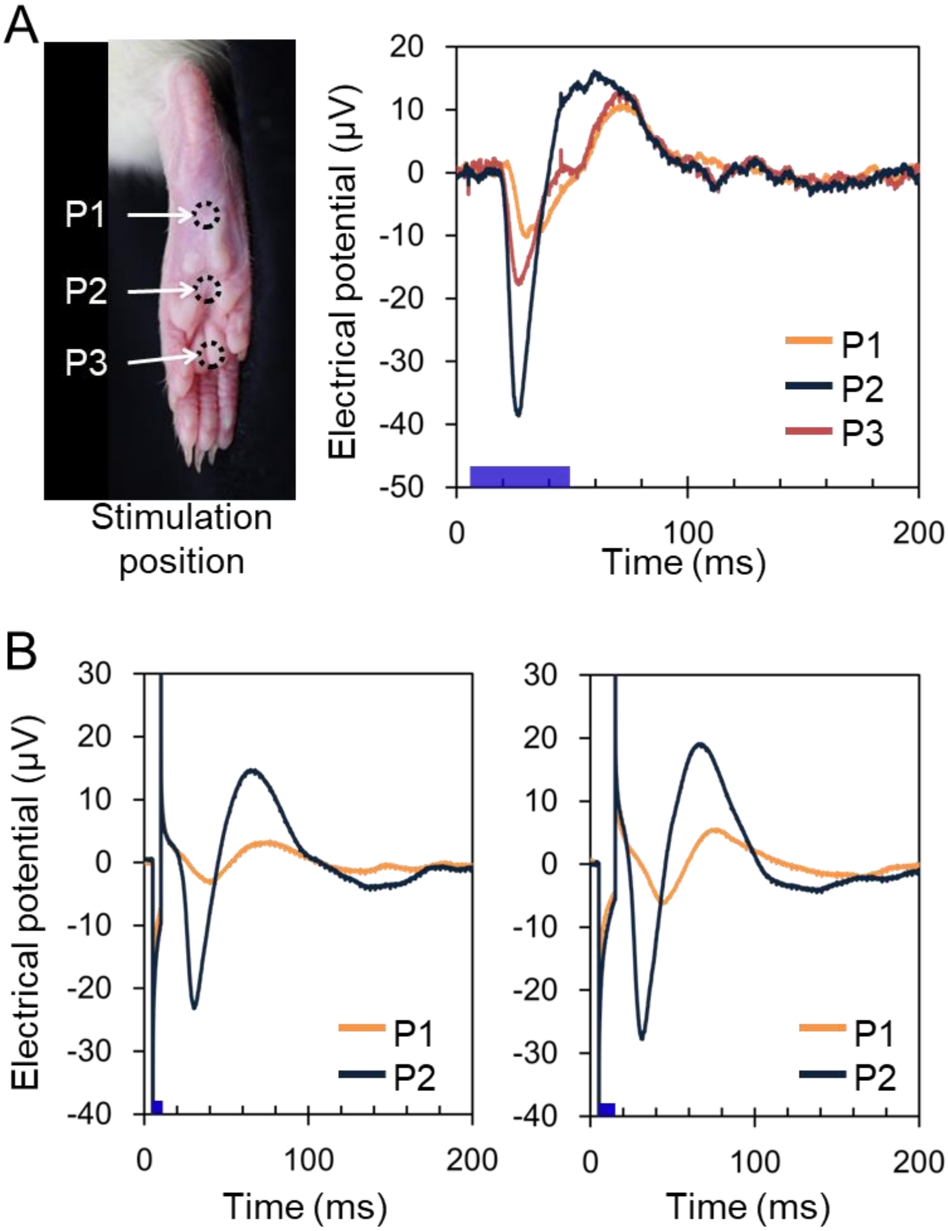

Fig. S6. SEPs evoked by optical stimulations. (**A**) The stimulations were delivered from a laser through an optical fiber. The optical power density was 24 mW/mm^2 at the tip of the optical fiber. Optical stimulations were delivered to the P1, P2, and P3 points. The SEPs were averaged over 300 stimulations. When the stimulation location was 10 mm from the position at which the maximum amplitude was recorded, the peak latency increased, and the amplitude decreased. (**B**) Displacement of the OLED by 10 mm from the maximally sensitive location results in the SEP exhibiting longer latency and lower peak amplitude. The blue bar indicates the period of optical stimulation. The longer stimulation duration of 10 ms (right) induces stronger SEPs than that of 5 ms (left).

Fig. S7. Evaluation of mechanical damage to the sciatic nerve caused by the implantations of optical devices. (**A**) The top photograph shows the prepared sham-operated animal. The middle photograph show the rigid cuff models simulating a conventional light emitting device. The OLED was prepared with a width of 5 mm along the sciatic nerve. (see materials and methods). Scale bar: 5 mm. (**B**) CD68 immunostaining results of the cross-sections of the sciatic nerves. The middle picture reveals that the sciatic nerve with a rigid cuff exhibited overexpressed CD68 owing to damage to the nerve. The nerve of the shame-operated and OLED-implanted group did not exhibit overexpression of CD68. Scale bar: 100 μm.

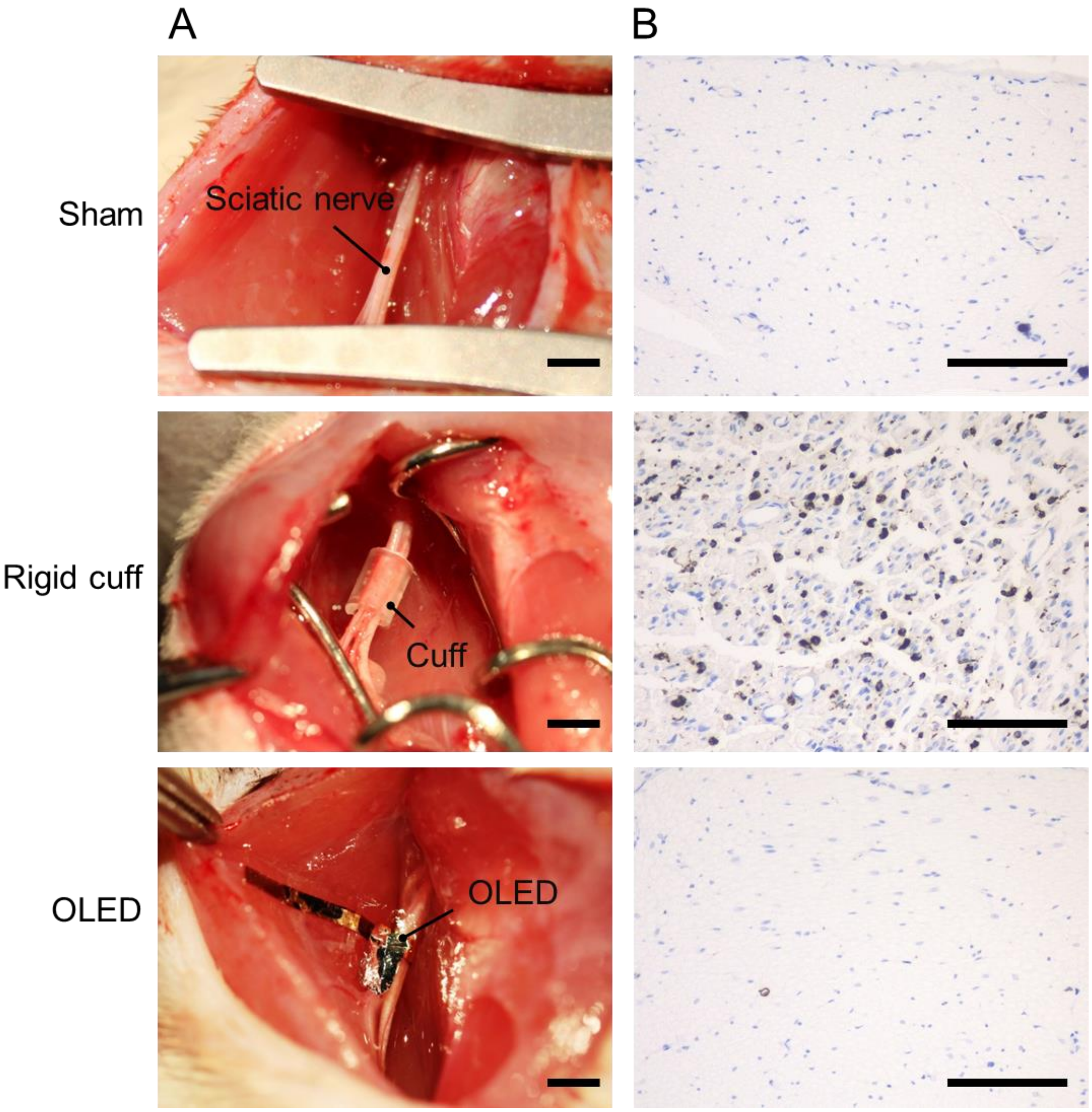

Fig. S8. Estimated attenuation of radio-frequency (RF) fields in the OLED for evaluating the MRI compatibility. (**A**) A simplified model of electromagnetic waves propagating through a conductive medium of thickness *t*. E_x and H_y are the electric and magnetic fields of the wave. E_{xi} is the incident electric field, and E_{xo} is the electric field at depth *t*. (**B**) Attenuation of RF field intensity due to the gold, aluminum, and ITO layers. The inset shows a magnified plot for the medium thickness of 1 μm.

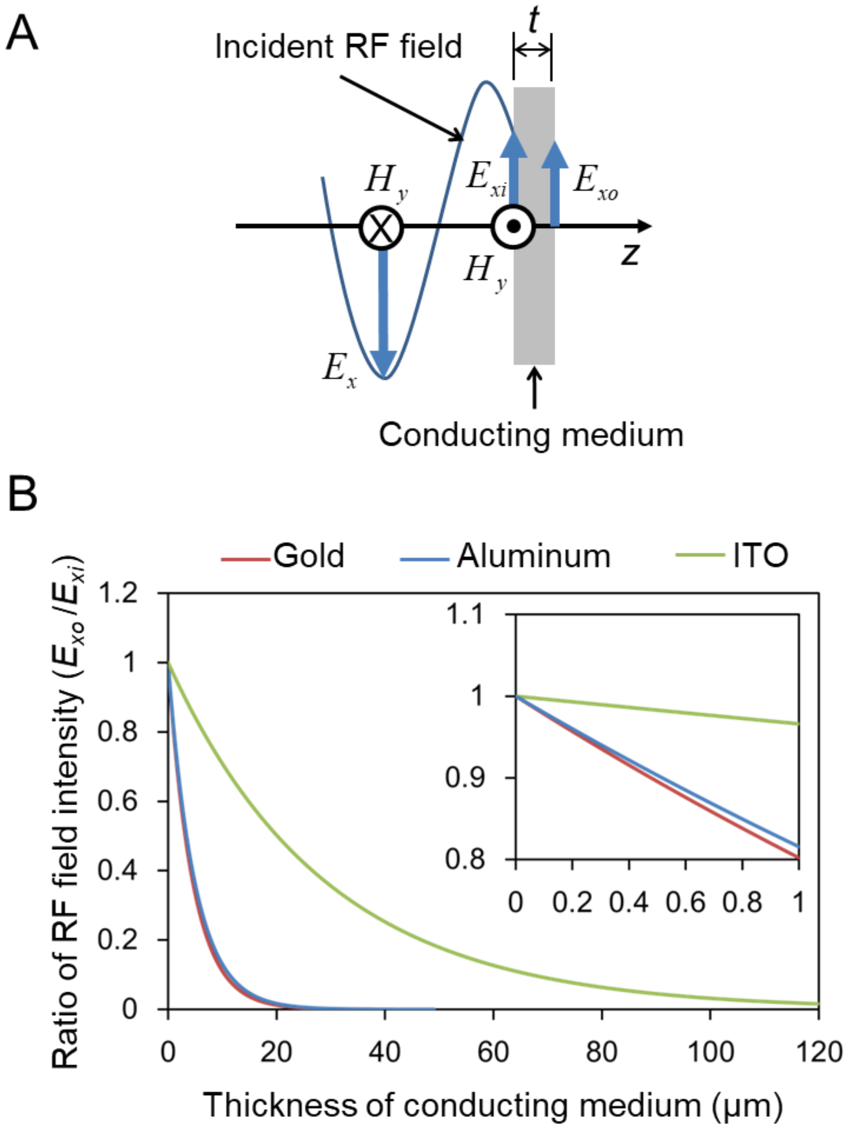

Fig. S9. Phantom experiments for evaluating the MRI compatibility of the OLED. (**A**) The left photograph shows an OLED sample immersed in a 1% agarose gel. The right image shows an enlarged portion of the MRI of this sample to show the region around the OLED cell. (**B**) The high MRI compatibility of the OLED means that the signal loss and image distortion are negligibly small. The signal intensity averaged over the area of the gold and ITO layers decreases by 7% compared to that of the Parylene only. The signal intensity decreases by 5% over the area of the OLED cell. In the aluminum-only area, the signal decreases by 3%. (**C**) Artifacts in MR images caused by two commercially available GaN LEDs (left : 1.6 mm × 0.8 mm, SML-310BATT86, ROHM Semiconductor, Japan; right : 2 mm × 1.25 mm, HSMR-C170, Broadcom Ltd., USA) inserted in a 1% agarose gel phantom. These samples were prepared consist only of iLEDs without any wiring components. The yellow arrows indicate boundaries of the MR signal loss areas. Scale bar, 5 mm.

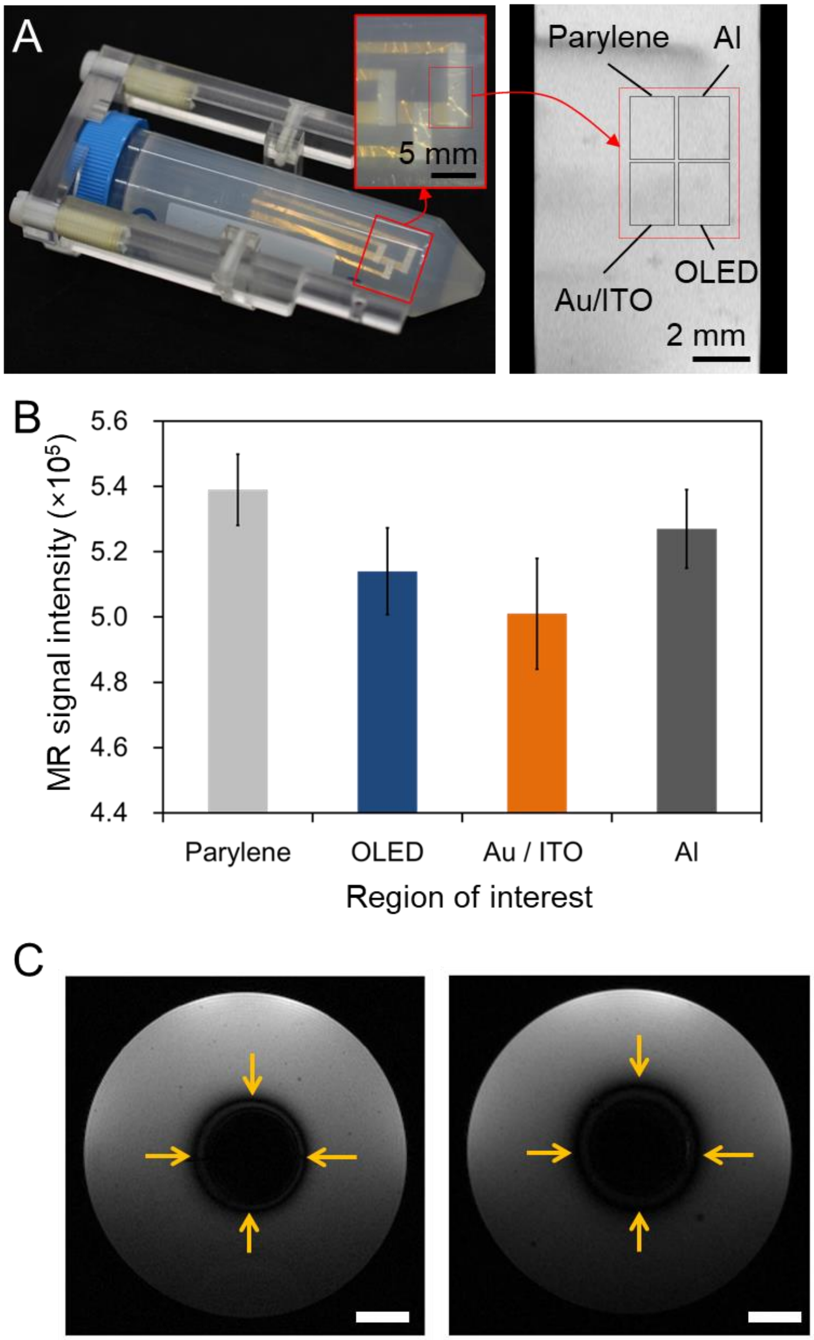

Fig. S10. Electrophysiological recording of muscle contractions induced by optical stimulations of the brain using the OLED. (**A**) Muscle contractions were observed in synchronization with the optical stimulations of 2 Hz on the motor cortex of the forepaw. (**B**) Evoked local field potentials at the surface of the brain by direct stimulations using the fiber-coupled laser and OLED. To avoid evoked wave deformation due to the OLED driving current, the illumination period of the OLED was adjusted to 60 ms.

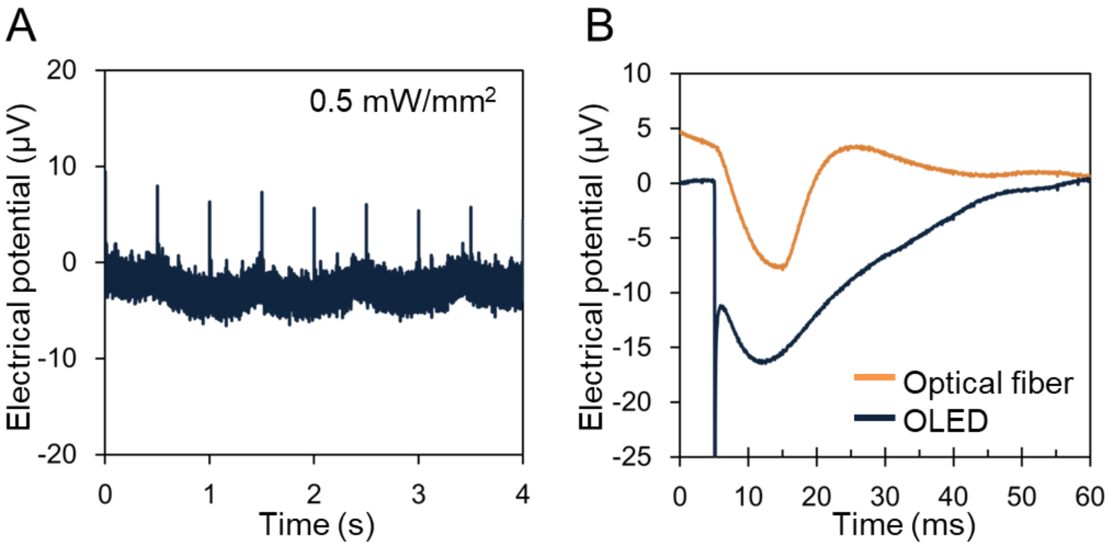

Fig. S11. Evaluation of thermal effect from the OLED at pulsed driving voltage mode. Rise in temperature caused by illumination of the OLED with pulsed driving voltage. The measurements were performed using a thermocouple.

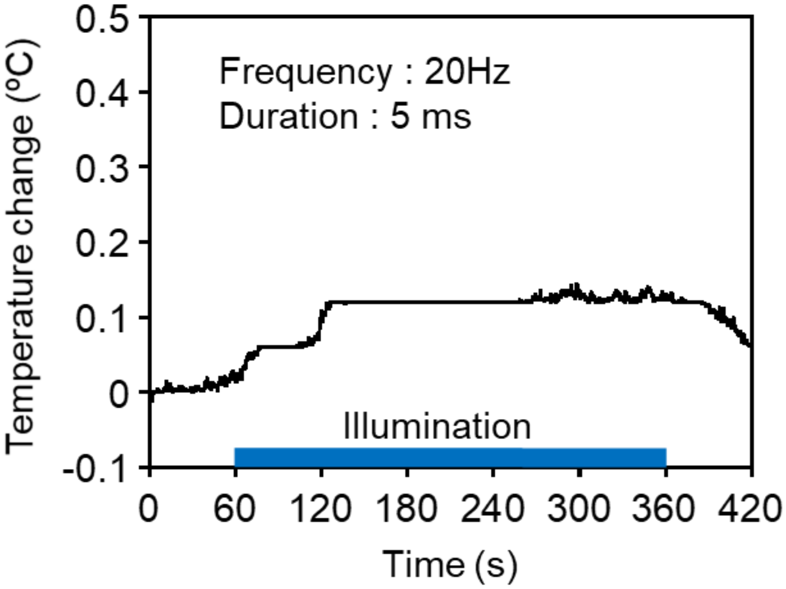

Fig. S12. Models for estimating the bending stiffness of devices. (**A**) The OLED conforms to the curved surface. (**B**) An array of rigid discrete LEDs distributed on the tissue. (**C**) A model for calculating the bending stiffness of a device with rigid discrete LEDs implemented on a flexible substrate.

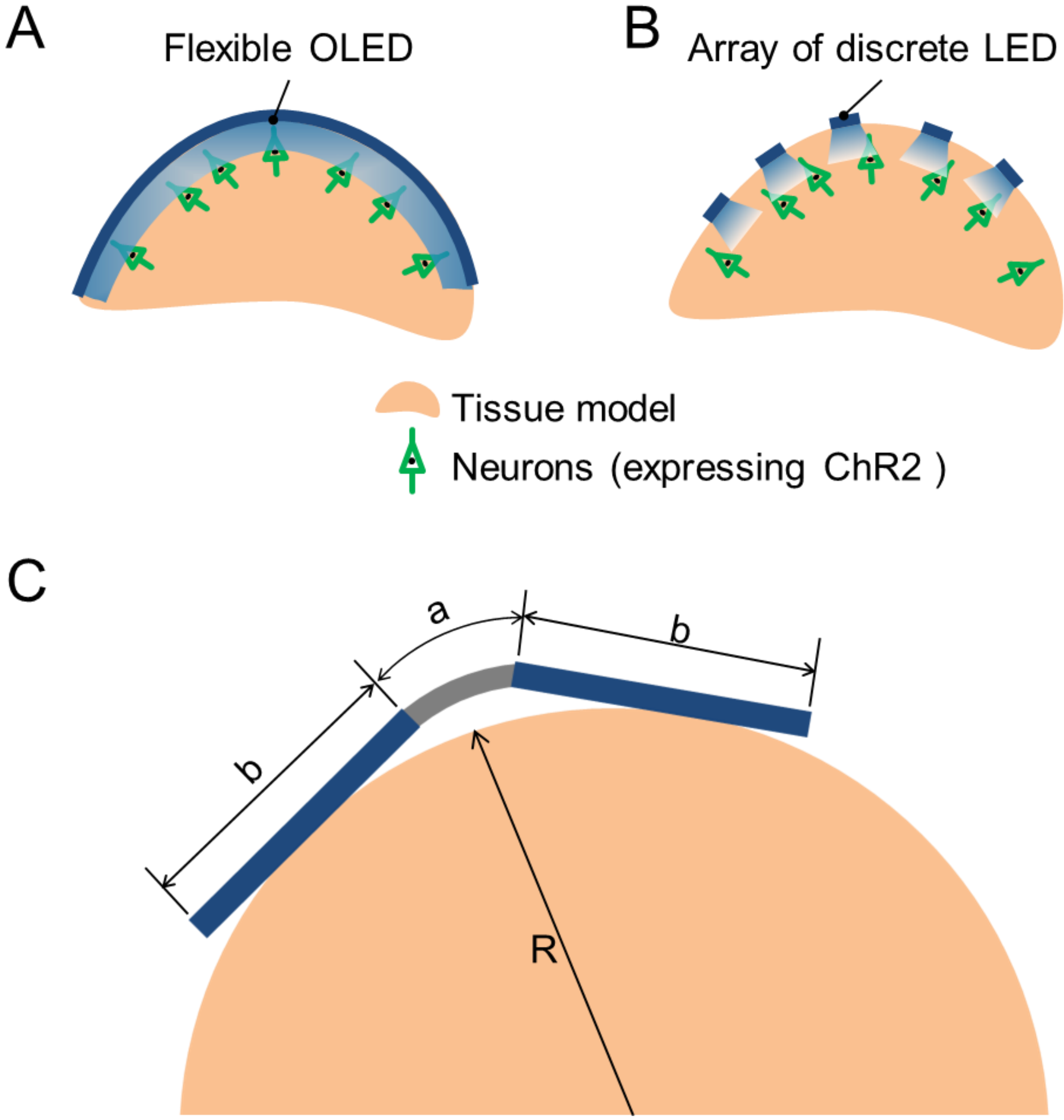

Table S1. Comparison of state-of-the-art optogenetic LED stimulators.

Materials	Substrate or encapsulation		Total thick.	Light intensity	Stimulation area	Temperature increase	MRI artifact	Ref
	Materials	Thick.						
Inorganic LED	Parylene	5 µm	75 µm	10 mW/mm^2	0.22 × 0.27 mm^2	0.3 ℃	-	1
	Polyimide / PDMS	3 µm / 100 µm	700 µm	10 mW/mm^2	0.22 × 0.27 mm^2	No change (40% duty)	-	2
	Stainless steel / PDMS	25 µm / 390 µm	700 µm	10 mW/mm^2	0.22 × 0.27 mm^2	1 ℃	-	3
Organic LED	PEN	125 µm	-	1 mW/mm^2	4 mm^2	0.3 ℃	-	4
	CMOS backplane (rigid)			1 W/m^2	20 mm^2 (based on 6 × 9 µm^2 pixel)	-	-	5
	Glass (rigid)			0.25-0.4 mW/mm^2	2.5 × 2.5 mm^2	-	-	6
	Parylene	1 µm	2 µm	0.4 mW/mm^2	2 × 2 mm^2	0.3 ℃	No artifact	This work

Movie S1 (separate file). Optical stimulation of gracilis muscle's nerve. Movement of rat's hindlimb by optical stimulations of the gracilis muscle nerve using the ultra-flexible OLED device. The stimulations were carried out at frequencies of 2, 5, and 10 Hz.

Movie S2 (separate file). Responses to optical stimulations of the sciatic nerve using the OLED. The optical stimulation induces stable contraction of the muscles.

Movie S3 (separate file). Recording of somatosensory evoked potentials by optical stimulations of the hindlimb using the OLED. The potentials were observed clearly for each optical pulse.

References

1. K. Y. Kwon, S. Member, B. Sirowatka, A. Weber, W. Li, Opto-microECoG Array: A Hybrid Neural Interface With Transparent Electrode Array and Integrated LEDs for Optogenetics. *IEEE Trans. Biomed. Circuits Syst.* **7**, 593–600 (2013).
2. K. L. Montgomery, *et al.*, Wirelessly powered, fully internal optogenetics for brain, spinal and peripheral circuits in mice. *Nat. Methods* **12**, 969–974 (2015).
3. A. D. Mickle, *et al.*, A wireless closed-loop system for optogenetic peripheral neuromodulation. *Nature* **565**, 361–365 (2019).
4. J. T. Smith, B. O'Brien, Y. K. Lee, E. J. Bawolek, J. B. Christen, Application of flexible OLED display technology for electro-optical stimulation and/or silencing of neural activity. *IEEE/OSA J. Disp. Technol.* **10**, 514–520 (2014).
5. A. Steude, E. C. Witts, G. B. Miles, M. C. Gather, Arrays of microscopic organic LEDs for high-resolution optogenetics. *Sci. Adv.* **2**, e1600061 (2016).
6. A. Morton, C. Murawski, S. R. Pulver, M. C. Gather, High-brightness organic light-emitting diodes for optogenetic control of Drosophila locomotor behaviour. *Sci. Rep.* **6**, 31117 (2016).